



This is a repository copy of *Nonlocal noise reduction method based on fringe frequency compensation for SAR interferogram*.

White Rose Research Online URL for this paper:
<https://eprints.whiterose.ac.uk/178328/>

Version: Published Version

Article:

Xu, H., Li, Z., Li, S. et al. (4 more authors) (2021) Nonlocal noise reduction method based on fringe frequency compensation for SAR interferogram. *IEEE Journal of Selected Topics in Applied Earth Observations and Remote Sensing*, 14. pp. 9756-9767. ISSN 1939-1404

<https://doi.org/10.1109/jstars.2021.3112588>

Reuse

This article is distributed under the terms of the Creative Commons Attribution (CC BY) licence. This licence allows you to distribute, remix, tweak, and build upon the work, even commercially, as long as you credit the authors for the original work. More information and the full terms of the licence here:
<https://creativecommons.org/licenses/>






Takedown

If you consider content in White Rose Research Online to be in breach of UK law, please notify us by emailing eprints@whiterose.ac.uk including the URL of the record and the reason for the withdrawal request.



eprints@whiterose.ac.uk
<https://eprints.whiterose.ac.uk/>

A Nonlocal Noise Reduction Method Based on Fringe Frequency Compensation for SAR Interferogram

Huaping Xu , Member, IEEE, Zhaohong Li, Shuo Li , Wei Liu , Senior Member, IEEE, Jingwen Li , Aifang Liu , and Wei Li

Abstract—Phase noise reduction is one of the key steps for synthetic aperture radar interferometry data processing. In this article, a novel phase filtering method is proposed. The main innovation and contribution of this research is to 1) incorporate local fringe frequency (LFF) compensation technique into the nonlocal phase filtering method to include more independent and identically distributed samples for filtering; 2) modify the nonlocal phase filter from three aspects: 1) executing nonlocal filtering in the complex domain of the residual phase to avoid gray jumps in phase, 2) adaptively calculating the smoothing parameter based on the LFF and the coherence coefficient, and 3) using the integral image in similarity calculation to improve the efficiency; 3) perform Goldstein filter in high coherence areas to reduce the computation expense. Experiments based on both simulated and real data have shown that the proposed method has achieved a better performance in terms of both noise reduction and edge preservation than some existing phase filtering methods.

Index Terms—Fringe frequency estimation, nonlocal filtering, phase noise reduction.

I. INTRODUCTION

SYNTHETIC aperture radar interferometry (InSAR) is an important technique for obtaining high-precision digital elevation model (DEM) and surface deformation of a wide area [1]. However, the existence of thermal noise, decorrelation, undersampling, and other factors will lead to various phase noise. The residual points caused by phase noise will reduce the success rate of phase unwrapping, and further affect the estimation accuracy of elevation and deformation. Therefore, how to effectively suppress the phase noise before phase unwrapping has been a focus of study in InSAR processing [2].

Phase filtering is the basic method to reduce phase noise, and its performance mainly depends on the number of pixels

involved in the filtering window. A larger filtering window has a better noise reduction effect when the pixels are independent and identically distributed (i.i.d) [3], otherwise, a large filtering window will lead to a serious loss of fringe details [4]. It is difficult to select an appropriate window size for steep terrain with dense and changeable fringes. Up to now, there are mainly two kinds of improved phase filtering methods for rough areas: adaptive window methods and local fringe compensation methods.

To balance the effects of noise reduction and fringe edge preservation, the adaptive window methods adjust the size, direction, or shape of the filtering window according to fringe density. When it is first presented in [5], eight predefined directional windows are used to match the phase fringes. The limited direction may mismatch the local fringe and lead to discontinuity in the filtered fringes. To match the filtering directional window with the fringes more accurately, in [6], the local tangents of the fringe edge are calculated first, and then the linear window along the tangential direction is interpolated to carry out low-pass filtering. The angle of the directional window can be chosen arbitrarily. However, for fringes with strong curvatures, the linear filtering window will cause some distortion to the curve fringe and make the phase fringe discontinuous. In [7], the directional filtering window consistent with the fringe direction is derived by tracking the tangential direction of the fringes, and the window size can be adjusted adaptively according to the stripe width. This method can keep the strong curvature fringes. However, the discontinuous fringe will affect the estimation of the direction and width of the filtering window. The intensity-driven adaptive-neighborhood method obtains similar pixels by using the intensity-driven region-growth technique and constructs a neighborhood with variable shape and size as the filtering window [8]. Irregular contour filtering windows can effectively improve their adaptability to steep terrain, but the limited number of neighborhood pixels will affect the performance of noise reduction.

Adaptive window filters can reduce the conflict between noise reduction and detail preservation to some extent. But it is very difficult to adjust the window size in an appropriate way, especially in rough areas with variable fringes. Another way to suppress phase noise in steep terrain is to reduce fringe density with local-fringe-compensation before noise filtering. A method proposed in [9] removes the local fringe frequency (LFF) and filters the residual phase in a local window, and finally adds back the removed fringes to the filtered residual phase. It can effectively reduce the fringe density and improve the edge-preserving

Manuscript received April 3, 2021; revised July 7, 2021 and September 6, 2021; accepted September 11, 2021. Date of publication September 14, 2021; date of current version October 8, 2021. This work was supported in part by the National Natural Science Foundation of China under Grant 61471020 and in part by Shanghai Aerospace Science and Technology Innovation Fund under Grant SAST2019-026. (Corresponding author: Shuo Li.)

Huaping Xu, Zhaohong Li, Shuo Li, and Jingwen Li are with the School of Electronic and Information Engineering, Beihang University, Beijing 100083, China (e-mail: xuhuaping@buaa.edu.cn; lizhaohong9712@buaa.edu.cn; shuo201@buaa.edu.cn; lijingwen@buaa.edu.cn).

Wei Li is with the Electronic and Electrical Engineering Department, University of Sheffield, S1 3JD Sheffield, U.K. (e-mail: w.liu@sheffield.ac.uk).

Aifang Liu is with the Nanjing Research, Institute of Electronics Technology, Nanjing 211113, China (e-mail: lafsx1997@163.com).

Wei Li is with the Shanghai Lizheng, Satellite Application Technology Company, Ltd, Shanghai 201100, China (e-mail: liwei20rth@139.com).

Digital Object Identifier 10.1109/JSTARS.2021.3112588

ability. To improve the LFF estimation accuracy, a statistical threshold is used to avoid sudden LFF changes in [10], while a further improved method is proposed in [11] by fusing multifrequency interferograms to improve the LFF-estimation accuracy. In [12], a complexity factor is introduced by combining the coherence coefficient, LFF, and residual point distribution, then the local fringe estimation window size is adaptively selected based on the complexity factor; as the residual phase is filtered by the Goldstein filter after removing the local fringe, the phase noise is effectively suppressed. The two-stage filtering method [13] separates the noisy phase into a smooth part and a detail part, where the smooth part is extracted from the filtered result in the first stage and the detail component is filtered in the second stage and then added to the smooth part to obtain the final result. These methods can protect the fringes while performing effective denoising, but their denoising performances are still limited because local neighborhood filtering windows are used.

Generally speaking, the more similar pixels used in phase filtering, the more accurate the phase estimation result. For those local filtering methods described above, their filtering windows cannot be too large; otherwise, it risks destroying phase details in the fringe-dense area and reducing the clarity of interferometric fringes; the estimation reliability is low when the noise level is high in the neighborhood filtering window. To overcome this issue, the nonlocal means filter (NLM) has been proposed for image denoising in recent years [14], [15]. NLM methods rely on the similarity of pixels rather than spatial proximity, so they can make use of similar pixels outside the neighborhood area to obtain a more accurate estimation value. To improve the reliability of similarity matching, the NLM determines the similarity of central pixels by matching their neighborhood patch (similarity window). The NL-InSAR method applies the NLM principle to interferometric phase processing [16]. It calculates the similarity based on the probability distribution of the interferometric phase, finds similar central pixels in the interferogram, and reduces noise by an averaging operation. It overcomes the restriction that the filtering window must cover a consecutive neighborhood. By making full use of similar pixels, it can maintain more detailed features after phase denoising. Although nonlocal filtering methods can use pixels in the whole image, the process is very time-consuming. Generally, a large local window (search window) is selected to reduce the computation load, and good denoising performance can be obtained as well [17].

For nonlocal filtering methods, the filtering effect is affected by the size of the similarity window. The phase difference of complex scenes is considered in the nonlocal-SAR filter for well-performing altitude map generation (NL-SWAG) [18], and the patch size is adaptively selected based on the heterogeneity of local scenes. The more intense the phase change in the searching window, the smaller the similarity window to be used. In [19], structure similarity (SSIM) and threshold are used to select similar pixels nonlocally to form the phase tensor from the interferogram, and then the Wiener filter is applied to reduce noise based on high-order singular value decomposition. An interferometric phase denoising method is proposed by combining local sparsity of wavelet coefficients and nonlocally patch similarity in [20]. These methods improve the accuracy of similarity estimation by

improving the similarity measurement method or adjusting the similarity window, so as to improve noise reduction. However, in steep terrain areas, the interferometric fringes are dense and vary greatly, which makes it difficult to select similar pixels and in turn limits its ability for noise reduction.

To reduce the adverse effects of phase fringes on similarity matching in steep terrains, a nonlocal filtering method based on LFF compensation is proposed in this article. First, the LFF is estimated and removed from the original phase to reduce fringe density in the search window; second, the residual phase is filtered by an improved nonlocal method; finally, the denoised phase is obtained by combining the filtered residual phase and the removed local fringe. The proposed method improves nonlocal filtering in the following aspects.

- 1) Noise reduction is carried out in the complex domain to further reduce the influence of interferometric fringes on the calculation of similarity weight.
- 2) The smoothing parameter is adaptively chosen on the LFF and the coherence coefficient of residual phase to preserve the fringes better.
- 3) The integral image is used in similarity calculation to improve operation efficiency.

The rest of this article is organized as follows. The principle and implementation process of nonlocal phase noise reduction based on fringe frequency compensation are presented in Section II. In Section III, results based on both simulated and real data are provided using the proposed method, in comparison with some existing local and nonlocal phase filtering methods. Conclusions are drawn in Section IV.

II. NONLOCAL NOISE REDUCTION METHOD BASED ON LOCAL FRINGE COMPENSATION

The filtering process of the nonlocal method involves more consistent pixels in a larger range. Compared with the local filters, it can suppress noise more effectively with less loss of fringe details. However, the dense and varied fringes reduce the number of similar pixels in steep terrain, which affects similarity matching and limits the noise suppressing ability. To reduce the influence of fringe on the matching of similar patches, we propose to compensate for the local fringe before nonlocal filtering and present the improved nonlocal filtering for the residual phase.

A. Nonlocal Filtering Principle

Through similarity matching, nonlocal filters can find more similar pixels for noise reduction. The procedure of similarity matching is shown in Fig. 1. By sliding the similarity window pixel by pixel in the search window, the similarity between patch x and patch y is calculated to determine the filtering weights of pixels in the search window. The filtered phase of NLM can be expressed as the weighted average of the pixels in the search window S , given by

$$NL(v(x)) = \sum_{y \in S} w(x, y) \cdot v(y) \quad (1)$$

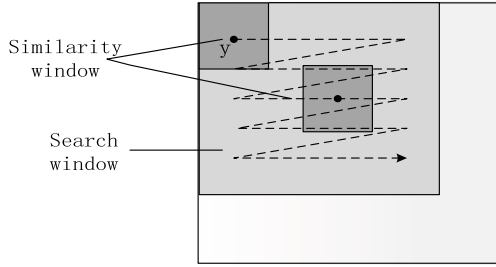


Fig. 1. Procedure of similarity matching.

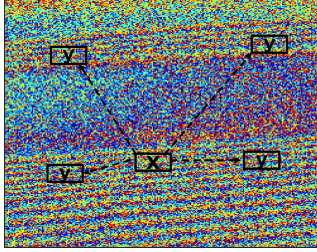


Fig. 2. Schematic diagram of similar patches.

where $v = \{v(x)|x \in I\}$ represents the phase of pixel x , and $w(x, y) \in [0, 1]$ is the weight depending on the similarity between surrounding patches around x and y with $\sum_{y \in S} w(x, y) = 1$.

In Fig. 2, pixels in red rectangles have similar structural features as those to be reconstructed. In the filtering process, the center pixels of these patches will have larger weights.

B. Principle of LFF Compensation

The interferometric phase noise is assumed to be additive [19], and the noisy phase can be expressed as

$$\varphi_n = \varphi_c + \varphi_r + n_0 \quad (2)$$

where φ_c is the prominent fringe phase which represents the basic topography, φ_r is the residual terrain phase, and n_0 is phase noise. φ_c represents the outline of terrain, which is the prominent component of the phase value. Therefore, the interferometric fringe density could be reduced by removing φ_c , and the residual phase φ_{res} , containing residual terrain and noise, can be represented as

$$\varphi_{res} = \varphi_n - \varphi_c. \quad (3)$$

The prominent fringe phase φ_c can be obtained by estimating the LFF.

$$\begin{aligned} & \varphi_c(m, n) \\ &= \arg \left\{ \sum_{i=1}^g C_i \exp [j2\pi (m f_{xi} + n f_{yi})] \right\}, g \in [1, G] \end{aligned} \quad (4)$$

where C_i is the amplitude of the frequency component (f_{xi}, f_{yi}) and G is the number of vectors. The LFF compensation effect is shown in Fig. 3. As can be seen, after removing the prominent fringe phase, the phase noise remains in the residual phase, and the fringe density in the residual phase is effectively reduced.

C. Nonlocal Noise Reduction Based on Fringe Frequency Compensation

1) *Fringe Frequency Removal*: To increase the number of similar pixels, it is proposed that the prominent fringe phase that causes significant fringes is removed from the noisy phase in the search window to reduce fringe density, and fringe frequency compensation is realized in the complex image, which is

$$I_{res}(m, n) = I(m, n) \cdot \exp[-j\varphi_c(m, n)] \quad (5)$$

where $I(m, n)$ is the complex form of the noisy phase, φ_c is estimated firstly, and then phase compensation is implemented by (5).

The phase values and similarities in a search window before and after removing LFF are shown in Fig. 4. From the similarities given in Fig. 4(b), (c), and (e), (f), it can be seen that the residual phase has sparser fringes, and more pixels with high similarity are obtained in the search window after removing the local fringes. With more similar pixels, phase estimation will become more accurate. Therefore, nonlocally filtering the residual phase is more reliable than directly dealing with the original phase.

2) *Adaptive Selection of Smoothing Parameter for Nonlocal Noise Reduction*: After removing local fringes, the residual phase is filtered using the improved nonlocal method. To further reduce the effect of the fringe boundary in the residual phase, all filtering operations are carried out in the complex domain. Euclidean distance has a good effect on patch matching in the case of additive Gaussian noise [20], so it is more suitable for measuring the similarity of interferometric phase in the complex domain than directly applying to the phase value under the assumption that the distribution of phase noise is complex Gaussian [21].

In the NL-InSAR method, the size of the search window and similarity window will affect the noise reduction performance. With the increase of search window size, the performance first becomes better and then worse [22]. This is because a larger neighborhood window contains more similar pixels, but as the window size continues to grow, the proportion of dissimilar pixels will increase. As to the similarity window, a smaller window has a better reduction effect on steep terrain, while a larger window has a better performance on flat terrain. In [22], the window size is optimized through iterative experiments, and finally, the search window and the similarity window are set to 17×17 and 7×7 , respectively. In our method, the size of the search window is adjusted to 21×21 because the fringes become sparser and the number of similar pixels increases after removing local fringes.

The value of the center pixel x after filtering is given as

$$\begin{cases} \bar{I}_{Re} = \sum_{y \in \text{Re}[I_{res}]} w_{Re}(x, y) \cdot v(y) \\ \bar{I}_{Im} = \sum_{y \in \text{Im}[I_{res}]} w_{Im}(x, y) \cdot v(y) \end{cases} \quad (6)$$

where $\text{Re}[I_{res}]$ and $\text{Im}[I_{res}]$ are the real and imaginary parts of the complex residual phase I_{res} . The weights $w_{Re}(x, y)$ and $w_{Im}(x, y)$ are determined by the Euclidean distance and smoothing parameters between the pixel patches centered on x

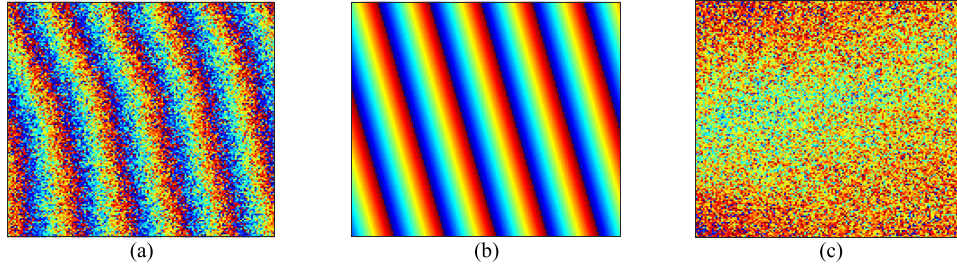


Fig. 3. Effect of LFF compensation. (a) Original phase. (b) Prominent fringe phase. (c) Residual phase.

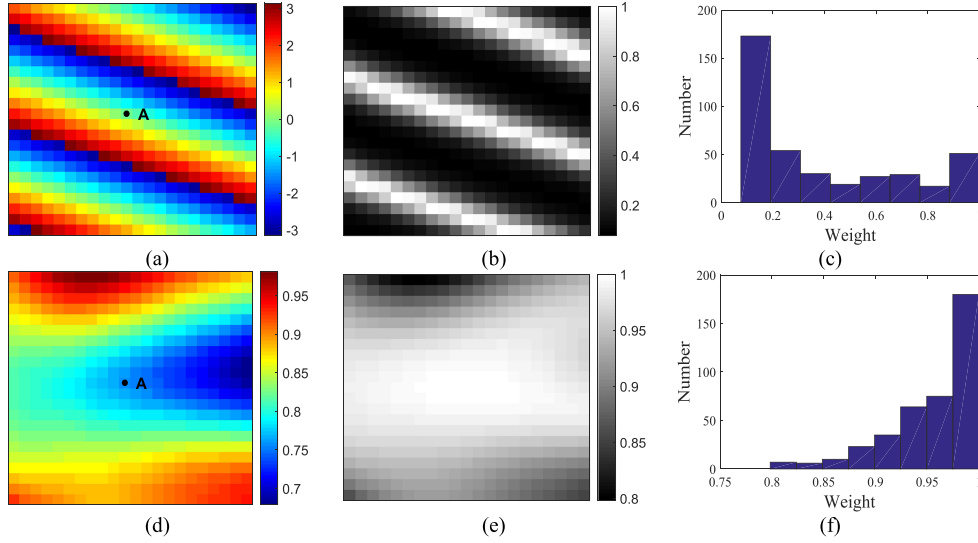


Fig. 4. Similarity changes before and after removing local fringes. (a) Original phase. (b) Similarity map of original phase. (c) Histogram of original phase similarity. (d) Residual phase. (e) Similarity map of residual phase. (f) Histogram of residual phase similarity. For better presentation, the similarity value is normalized.

and y

$$w_{\text{Re,Im}}(x, y) = \frac{\exp(-\|V(x) - V(y)\|_{2,\alpha}^2/h^2)}{\sum_y \exp(-\|V(x) - V(y)\|_{2,\alpha}^2/h^2)}$$

$$x, y \in \text{Re}[I_{\text{res}}], \text{Im}[I_{\text{res}}] \quad (7)$$

where $\|\cdot\|_{2,\alpha}^2$ is the Gaussian weighted Euclidean distance, and the Gaussian kernel is

$$G(\Delta x) = \frac{1}{2\pi\sigma^2} \exp\left(-\frac{\Delta x^2}{2\alpha^2}\right) \quad (8)$$

where $\alpha > 0$ is the standard deviation of the Gaussian kernel. Δx represents the distance between the pixel in the similarity block and its center pixel, which highlights the contribution of the center pixel of the similarity block to the similarity calculation. h is the smoothing parameter, which controls the attenuation speed of the weight function. The larger the value of h , the more obvious the smoothing effect of phase filtering.

In the smooth region, the number of similar pixels is large, and a larger h is required, which gives a small range of weights and suppresses the noise well. On the contrary, in the rugged

region, the number of similar pixels is small, a smaller h is needed to increase the weights difference so that similar pixels would have larger weights to preserve the detailed textures. In literature, the smoothing parameter h is mostly determined according to the noise distribution and the size of the search window. In [20], the value of h is directly proportional to the standard deviation of noise σ_n , with $h \approx 10\sigma_n$, while it is found that better noise reduction is achieved when the value of h is within the range $0.4 - 0.6\sigma_n^2$ in [23]. These methods only consider the distribution of noise in the search window. For the interferometric phase, both noise statistics and fringe density should be considered. In our method, the adaptive smoothing parameter h' is chosen adaptively as

$$h' = 10\sigma_n \cdot \gamma \cdot (1 + f'_x{}^2 + f'_y{}^2)^{-1/2} \quad (9)$$

where γ is the coherence value and (f'_x, f'_y) is the dominant frequency of the residual phase. The value range of $\gamma \cdot (1 + f'_x{}^2 + f'_y{}^2)^{-1/2}$ is within $(0, 1)$. σ_n is the standard deviation of phase noise in the search window.

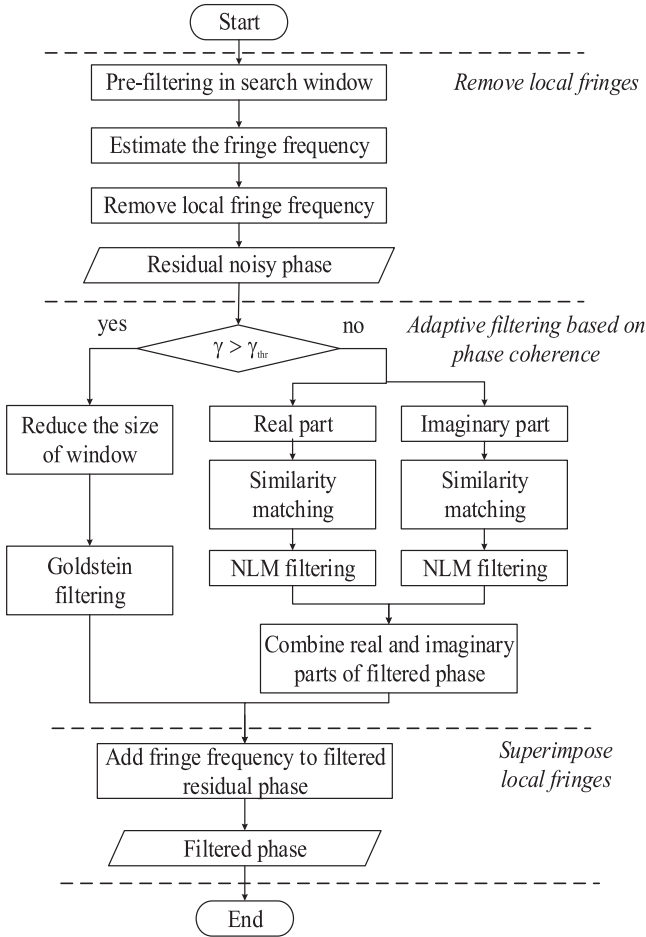


Fig. 5. Flowchart of the proposed phase filtering method.

The variance of phase noise can be expressed as a function of coherence γ [24]

$$\sigma_n^2 = E[(\phi - \phi_0)^2] = \begin{cases} \frac{\pi^2}{3} - \pi \arcsin \gamma + \pi \arcsin^2 \gamma - \frac{L_{i_2}(\gamma^2)}{2}, & L = 1 \\ \int_{-\pi}^{\pi} (\phi - \phi_0)^2 pdf(\phi; \gamma, L, \phi_0) d\phi, & L \geq 2 \end{cases} \quad (10)$$

where $L_{i_2}(\cdot)$ represents the Euler logarithm with base 2 and L is the number of observations.

3) *Method Implementation*: The implementation of the proposed nonlocal phase noise reduction method based on local fringe compensation is shown in Fig. 5.

Step1: Remove local fringes

In a search window, the LFF can be estimated with different methods. For example, the linear fringe estimation with the autocorrelation function method, the maximum likelihood method (ML) [25], or the modified multiple-signal classification method [26], and the nonlinear fringe estimation with prominent spectrum extraction method [27]. Given the stability of the ML method, it is used to estimate the LFF here. After the interferometric phase is transformed into the frequency domain by 2-D fast Fourier transform (FFT2), the LFF is derived

by detecting the amplitude peak position of the 2D signal spectrum

$$\max_{(\hat{f}_x, \hat{f}_y)} \left(\sum_{x=k-p}^{k+p} \sum_{y=l-q}^{l+q} \exp[j\varphi_n(m, n)] \cdot \exp[-j2\pi(m\hat{f}_x + n\hat{f}_y)] \right). \quad (11)$$

To reduce the error caused by the quantization of FFT, the Chip-Z transform [28], [29] is used to further improve the accuracy of fringe frequency estimation. The frequency estimation offset is obtained by 32 times sampling of Chip-Z transform to correct the frequency estimation result. Then the linear prominent fringe phase is expressed as

$$\varphi_{c1}(m, n) = 2\pi(m\hat{f}_x + n\hat{f}_y). \quad (12)$$

In areas with large fringe curvature, it is difficult to use linear fringes to compensate for the fringes in the search window. In this case, we use the prominent spectrum extraction method to estimate the prominent fringe. According to (4), a certain number of vectors with larger weight C_i are selected to form the main phase component, and the residual phase vector reflects terrain details and phase noise.

The prominent frequency spectrum can be obtained by the following rule:

$$S'(u, v) = \begin{cases} S(u, v), & |S(u, v)| \geq b \\ 0, & |S(u, v)| < b \end{cases} \quad (13)$$

where $S(u, v) = F[I_n(m, n)]$ is the phase spectrum of the search window. b is the spectrum amplitude threshold. In this article, b is determined by the lower bound of the first 3% maximum spectrum amplitude. In comparison with the half power point threshold given in [27], the proposed adaptive spectrum amplitude threshold is beneficial to estimate the main fringes more precisely. Fig. 6 shows the phase fringes extracted by different thresholds. In each group of images, the left one is the interferometric phase and the right one is the corresponding spectrum. It can be seen from Fig. 6(b) that the threshold set according to the half power point is too high, and only a small amount of useful spectrums is extracted and detail information is lost. The result by the proposed method shown in Fig. 6(c) retains the prominent spectrum sequence according to the number of points in the FFT window, which can avoid the influence of extreme spectrum amplitude on threshold selection and extract the prominent fringe more effectively.

Then the nonlinear prominent fringe phase is expressed as

$$\varphi_{c2}(m, n) = \arg\{F^{-1}[S'(u, v)]\}. \quad (14)$$

The residual phase in the complex domain is obtained by (5).

The nonlinear method can remove the local fringe better, but the estimation result is susceptible to phase noise. Therefore, when the distribution phase fringes are simple, the linear fringe estimation method can be used to compensate for the local phase. On the other hand, it is more suitable to compensate for nonlinear

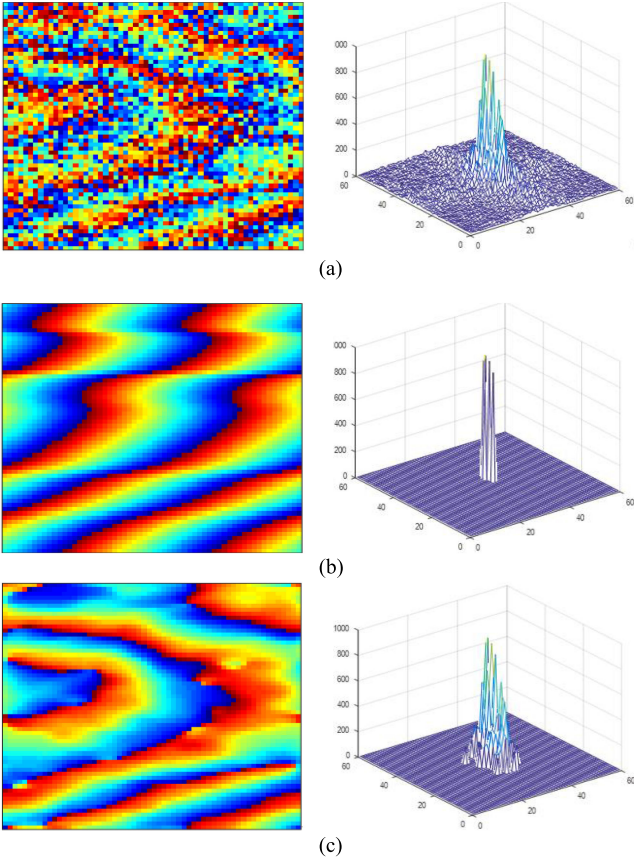


Fig. 6. Prominent fringes extracted by different thresholds. (a) Original noisy phase. (b) Half power point as the threshold. (c) Retaining 3% of the maximum amplitude spectrum.

fringes using method 2, when the curvature of phase fringe is large and the phase noise is not too heavy.

Step2: Adaptive filtering based on phase coherence

In a region with high coherence, the traditional local filtering method can also obtain good filtering results. To improve the operation efficiency, nonlocal filtering is only applied in the low coherence region, while the local filtering method, Goldstein filtering method used in this article, is applied in the high coherence region. The coherence γ can be calculated by the following formula [2]:

$$\gamma = \frac{E[S_1 S_2^*]}{\sqrt{E[|S_1|^2] E[|S_2|^2]}} \quad (15)$$

where S_1 and S_2 are the main and slave SAR complex images, respectively, and $E[\cdot]$ is the mathematical expectation. Set the local filtering window size to 1/2 of the search window and perform Goldstein filtering when the average coherence in the search window is higher than the threshold value. (threshold is set as 0.7 in this article); otherwise, the residual phase in the search window is filtered nonlocally. The nonlocal filtering process is carried out in the complex domain of the phase. The residual phase is filtered using the similarity of the real part and the imaginary part, separately, and the filtered residual phase is obtained by combining the filtered real and imaginary parts.

TABLE I
PARAMETERS FOR SIMULATED DATA

Parameter	Value
Baseline	600m
Wavelength	0.0313m
Near range	630km
Baseline obliquity angle	10°
Slant range resolution	2.3m
View angle	30°

The integral image method proposed in [30] is employed to calculate the similarity to reduce the operation cost. The value of each point in the integral image is the sum of all the pixel values in the upper left corner of the original image. The sum of all pixels in the similarity window can be quickly calculated by searching through the integral image four times. The complexity of the algorithm for calculating Euclidean distance has been reduced from $O(ND^2d^2)$ to $O(ND^2)$ for an image with N pixels, where D is the size of the search window and d is that of the similarity window.

Step 3: Superimpose local fringe

After residual phase filtering, the filtered phase is obtained by combining the removed local fringe with the filtered residual phase

$$\bar{\varphi}(m, n) = \arg \{ \bar{I}_{res} \cdot \exp [j\varphi_c(m, n)] \}. \quad (16)$$

Specifically, the local fringe is added back to the complex domain. Then, the interferometric phase is obtained by taking the angle of the complex value.

III. RESULTS AND ANALYSIS

In this section, both simulated and real data are filtered with different methods and the results are evaluated. Two local filtering methods, including the slope adaptive method and the Goldstein filtering method, and two nonlocal filtering methods, including the NL-InSAR [16] and the NL-SWAG [18] methods, are used as comparisons. All the experiments are implemented on a PC with Intel(R) Core(TM) i5-5200U@2.2GHz CPU and a 32-GB memory.

A. Simulated Data

The simulated SAR image is generated using real DEM in Xi'an, China, and the main parameters are listed in Table I.

The clean wrapped phase can be expressed as

$$\varphi = \text{mod} \left(\frac{2\pi \cdot \Delta r}{\lambda}, 2\pi \right) - \pi \quad (17)$$

where λ is the wavelength, Δr is the range difference calculated by DEM and satellite position, and $\text{mod}(\cdot, 2\pi)$ denotes the residue value after dividing by 2π .

A pair of SAR complex images are simulated with the method in [31] while random phase noise and complex Gaussian noise are added. The noisy wrapped phase is obtained by conjugate cross-product of main and slave complex images. The simulated

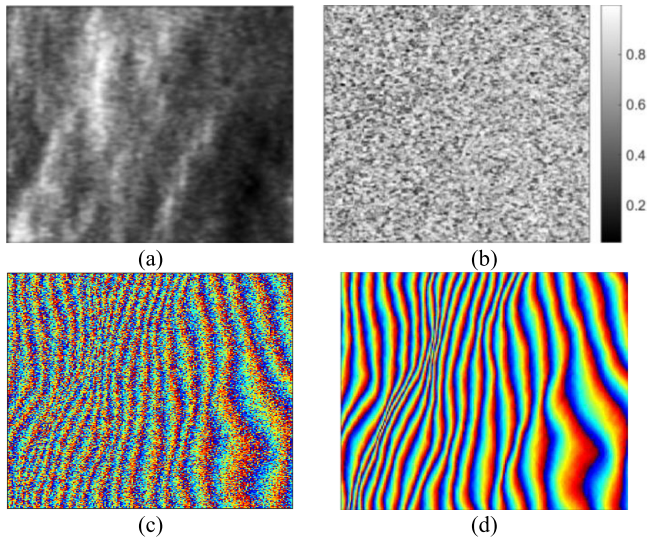


Fig. 7. Simulated data. (a) SAR image. (b) Coherence map. (c) Interferometric phase. (d) Clean wrapped phase.

results are shown in Fig. 7, and the image size is 290×200 pixels.

The local filtering methods used in the test are slope adaptive filter and Goldstein filter, and the filtering window size is 13×13 . The filtering parameter of Goldstein filter is set as $1 - \gamma$ [35]. Nonlocal filtering methods are the NL-InSAR method, NL-SWAG method, and the proposed method with a search window of 21×21 and a similarity window of 7×7 . The proposed method1 uses the ML method to estimate linear fringes, while the proposed method2 uses spectrum amplitude extraction method to estimate prominent fringes. The results of the different filtering methods are shown in Fig. 8, where the left image is the filtered result, and the right one shows the phase estimation error and the distribution of residual points, with purple dots representing positive residuals and cyan ones negative residuals.

As can be seen from the figures above, in Fig. 8(a), the slope adaptive filter performs well in fringe-sparse areas, but it generates more residual points in fringe-dense areas. In Fig. 8(b), the Goldstein filter blurs fringe boundary and introduces phase distortion. In Fig. 8(c), there are obvious fringe ruptures that will lead to severe error in the following phase unwrapping operation. Intuitively, both the NL-SWAG method and the proposed method shown in Fig. 8(d)–(f) can effectively suppress the phase noise. It can be seen from the phase error diagrams that the error and residual points of the proposed method2 are less than other methods not only in areas with sparse fringes but also in areas with dense fringes. In order to compare the denoising performance of different methods, the phase error profiles of different filtering results in area A and area B are shown in Fig. 9.

As can be seen from Fig. 9, in area A with dense fringes, the two local filtering methods, i.e., slope adaptive filtering and Goldstein filtering, have a large phase error. This shows that the local filtering window cannot effectively suppress the phase noise because only a limited number of pixels are used for phase

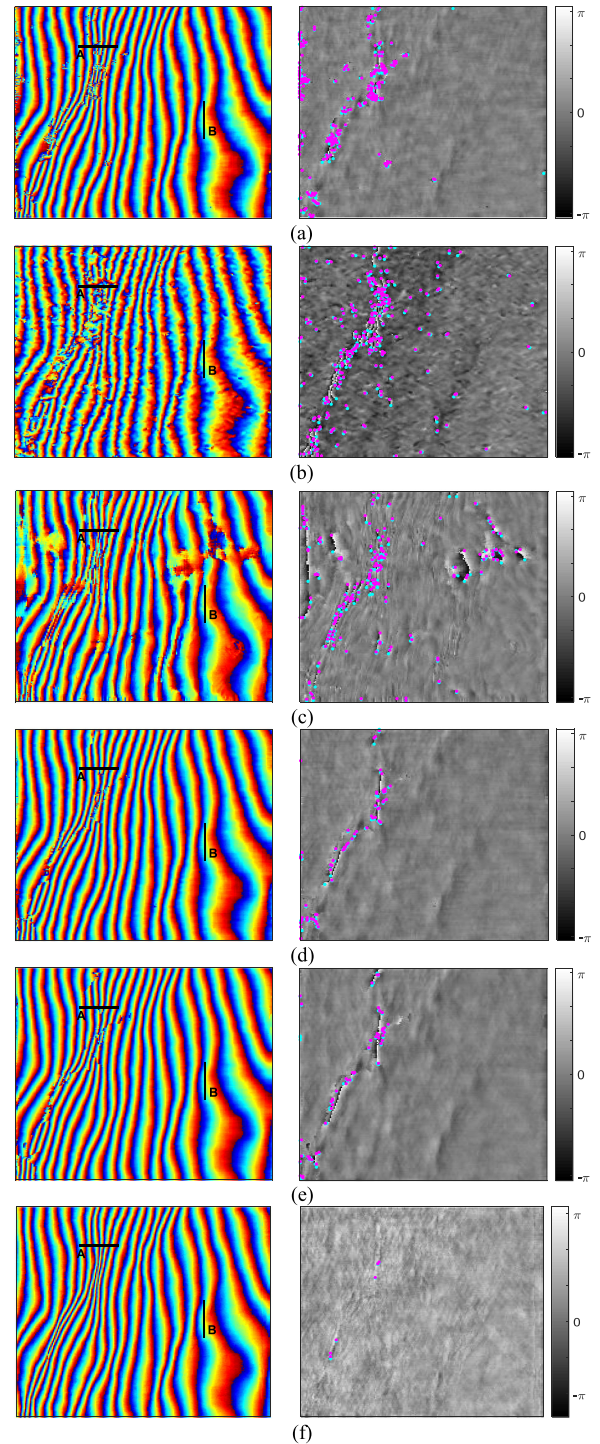


Fig. 8. Filtered phase and phase error. (a) Slope adaptive filtering. (b) Goldstein filtering. (c) NL-InSAR. (d) NL-SWAG. (e) Proposed method1. (f) Proposed method2.

estimation. The three nonlocal methods, i.e., NL-InSAR, NL-SWAG, and the proposed method, have better noise reduction effects. This is because nonlocal filters use more information in a larger search window, thereby having a more stable noise reduction performance. In area B with sparse fringes, most methods have achieved good noise reduction results, while the Goldstein

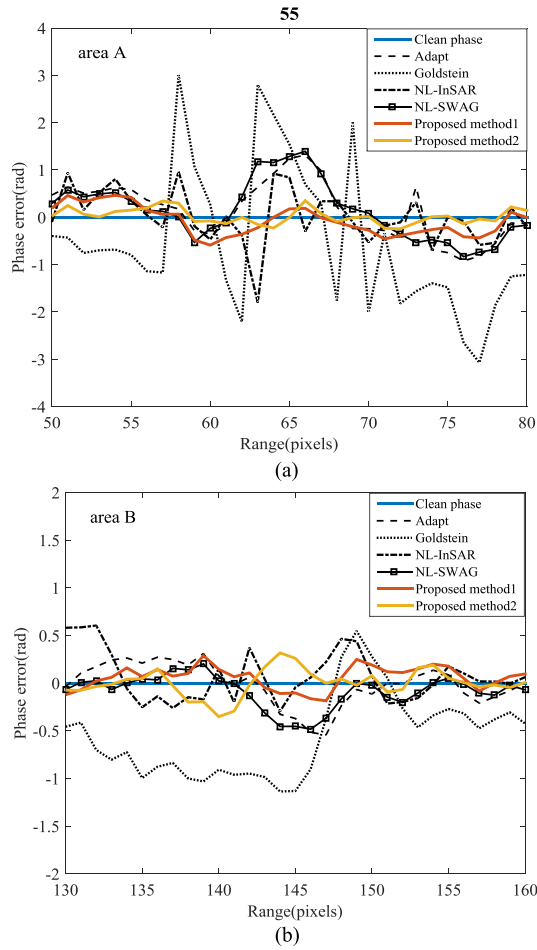


Fig. 9. Cross-sections of phase error. (a) Area A. (b) Area B.

filter has larger phase errors. Goldstein filtering in the frequency domain tends to remove the high-frequency information as noise and has poor ability in preserving phase details. Compared with the proposed method, the similarity matching of NL-InSAR is interfered by phase fringes, resulting in a reduction in the number of similar pixels, and therefore its noise reduction effect is not significantly improved. The NL-SWAG method adaptively selects the size of the matching window. The window is small where the fringes are dense and the similarity estimation is less reliable because the small window is sensitive to phase noise. The proposed methods can use a larger similarity window after removing local fringes and can select similar pixels more accurately. It is obvious from Fig. 9 that in areas with dense fringes or changeable fringes, more improvement is achieved by the proposed method than that in areas with sparse fringe.

To quantitatively compare the filtering results of different methods, phase root mean square error (RMSE), edge-preserving index (EPI), the number of residual points and filtering time, are introduced to evaluate the filtered phases. Their definition can be found in [32].

The evaluation results are shown in Table II. It can be seen from the results that the slope adaptive filter has a smaller phase RMSE and its EPI is close to 1, which is because the LFF compensation operation can protect the fringe edge and reduce

TABLE II
EVALUATION RESULTS OF SIMULATED DATA

Interferogram	Residues	EPI	Phase RMSE (rad)	Elevation RMSE (m)	Time (s)
Noisy phase	12595	2.985	1.301	3.25	/
Slope adaptive filter	432	1.064	0.396	0.99	170
Goldstein filter	445	1.159	0.842	2.11	71
NL-InSAR	342	1.061	0.564	1.41	45
NL-SWAG	119	1.013	0.459	1.15	96
Proposed method1	105	0.997	0.373	0.93	191
Proposed method2	12	1.003	0.193	0.48	124

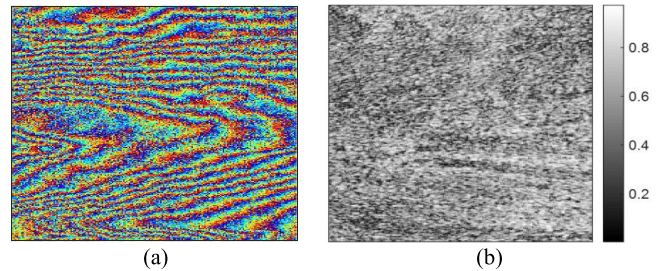


Fig. 10. Real data. (a) Interferometric phase. (b) Coherence map.

the phase error. Nonlocal methods can use more similar pixels to suppress noise so that they have fewer residues. The proposed methods have the advantages of both LFF compensation and nonlocal filtering, so they have not only have better noise suppression ability but also better edge preservation ability. However, one disadvantage of the proposed method is that due to the high computational complexity in similarity matching, the running time increases significantly. To show the filter performance more intuitively, according to the height ambiguity of the system, the elevation accuracy of the DEM inverted by different interferometric phase is derived [2] and shown in the fourth column of Table II. Since nonlinear frequency estimation can compensate the local fringes more effectively, the filtered result of the proposed method2 has the minimum phase error. It is worth noting that the proposed method2 is more efficient than proposed method1 because chip-z transformation is not needed in nonlinear fringe estimation.

B. Real Data

1) *ERS SAR Data*: The real SAR image data is from the ERS satellite recording in September 2000 and October 2000 at the Enta volcano in Italy. The selected area has 400×220 pixels. The fringe pattern and coherence map are shown in Fig. 10. Due to volume scattering decorrelation and temporal decorrelation caused by vegetation growth, the average coherence coefficient of the selected region is only 0.537.

Slope adaptive filtering, Goldstein filtering, NL-InSAR, NL-SWAG, and the proposed method are used to filter the phase in Fig. 10(a). The filter parameters are the same as those in Section III-A. The filtering results of different methods are shown in Fig. 11. In each row, the left image is the denoised

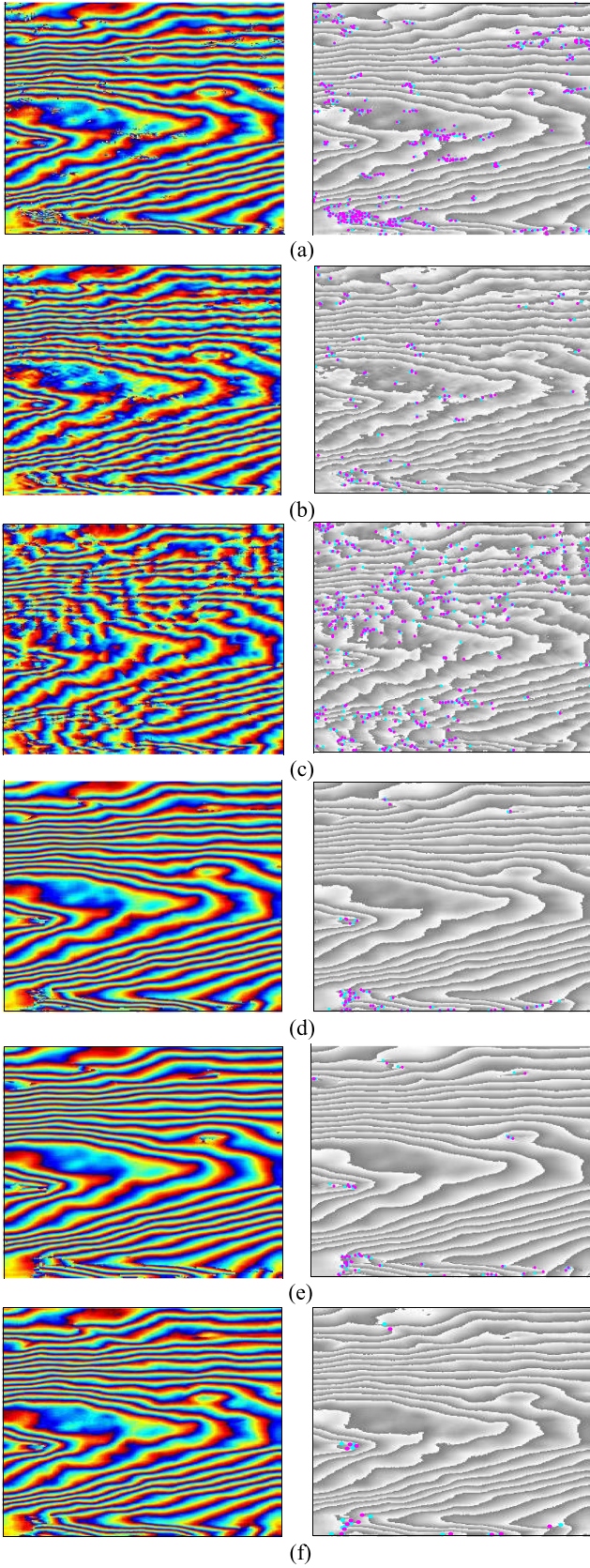


Fig. 11. Filtered phase and residues distribution. (a) Slope adaptive filtering. (b) Goldstein filtering. (c) NL-InSAR. (d) NL-SWAG. (e) Proposed method1. (f) Proposed method2.

TABLE III
EVALUATION RESULTS OF ERS DATA

Interferogram	Residues	RPSD	Time(s)
Noisy phase	15170	1.532	/
Slope adaptive filter	869	0.597	213
Goldstein filter	169	0.626	91
NL-InSAR	722	0.749	87
NL-SWAG	97	0.782	172
Proposed method1	88	0.358	339
Proposed method2	29	0.281	248

phase, and the right one is the distribution map of residual points. In the right figures, the purple dots represent positive residual points, while the cyan points represent negative ones. Since the phase error cannot be calculated using real data, the denoised phase is used as the gray background in the right image to show the position of residual points.

The low coherence in this vegetation coverage area makes it difficult to obtain a large number of i.i.d. samples in a local window for interferometric noise suppression [33]. The proposed methods employ LFF compensation and nonlocal strategy to look for more i.i.d. pixels in a larger range and reduce the weight of heterogeneous pixels to improve denoising performance. In Fig. 11(a), many residual points are left in the result of the slope adaptive filtering method. In Fig. 11(b), the Goldstein filtering method produces phase ambiguity when the filtering intensity is too high. In Fig. 11(c), there are some fringe breaks and distortions in the results of the NL-InSAR method. In Fig. 11(d), the result of the NL-SWAG method has more residual points than the proposed methods. In Fig. 11(e), the proposed method can use a larger matching window after removing local fringes and has better noise reduction and fringes preservation compared with the NL-SWAG method. As shown in Fig. 11(f), the fringes are most complete and clear, and the edge information and details are preserved best. Similarly, SAR interferograms in urban areas are more heterogeneous and the proposed methods also perform better for them.

Due to the lack of noiseless real data, MSE and EPI of the filtered phase cannot be calculated. Thus, the performance of the filtering results is evaluated with the number of residual points, residual phase deviation (RPSD) and filtering time. The RPSD is calculated after removing the local fringes, whose definition and calculation formula can be found in [32].

The evaluation results are shown in Table III. The empirical conclusion is similar to that of the simulated data. Slope adaptive filtering and NL-InSAR have more residual points. Goldstein filter has better noise reduction ability but cannot keep the edge and detailed information well. The proposed method has the least residues and RPSD, so it has achieved the best results in both residual point reduction and fringe preservation, which facilitates better the following phase unwrapping and elevation inversion. But the proposed method spends more running time because both LFF compensation and similarity matching have a large amount of calculation.

2) *NSAR Data*: Another set of airborne data over a mountain area in Weinan, Shaanxi Province recorded by N-SAR system in

TABLE IV
SYSTEM PARAMETERS OF N-SAR

Parameters	Value
Baseline	3.7m
Wavelength	0.0312m
Near range	10.2km
Baseline obliquity angle	0.005°
Slant range resolution	0.3m
Azimuth resolution	0.5m
Flight height	8.0km
Platform speed	117.6m/s

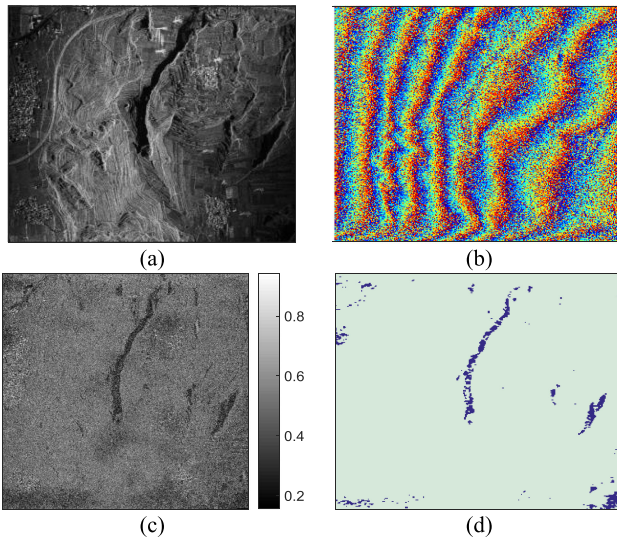


Fig. 12. NSAR data. (a) SAR amplitude image. (b) Interferometric phase. (c) Coherence map. (d) Shadow label.

January 2021, is selected to demonstrate the effectiveness of the proposed method. NSAR is an airborne SAR/InSAR system developed by Nanjing Research Institute of Electronic Technology [34]. The main parameters of NSAR systems are shown in Table IV. The amplitude image, interferometric fringes, coherence map of size 300×300 pixels are shown in Fig. 12(a)–(c). At the center of the scene, the slope of a gully area is large, resulting in obvious shadows. Shadow areas lack useful information and have a low correlation coefficient. They are detected and labeled as Fig. 12(d).

The results of different filtering methods are shown in Fig. 13. Since the airborne data has sparse stripes, all filtering methods have achieved good noise reduction effects. Among them, the results of NL-SWAG and the proposed method are slightly better than the other three methods. In Fig. 13(d), pixels in the shadow area are over-filtered by the NL-SWAG method, leading to artifacts, which will fail to reflect the real terrain in the final height estimation result. The proposed method improves the accuracy of similarity calculation after frequency compensation and therefore can suppress noise well in the normal area and retain the shadow boundary. By examining the bottom area of the filtered phase, it can be found that among the five filtering methods, only the proposed one can keep the fringes intact, while

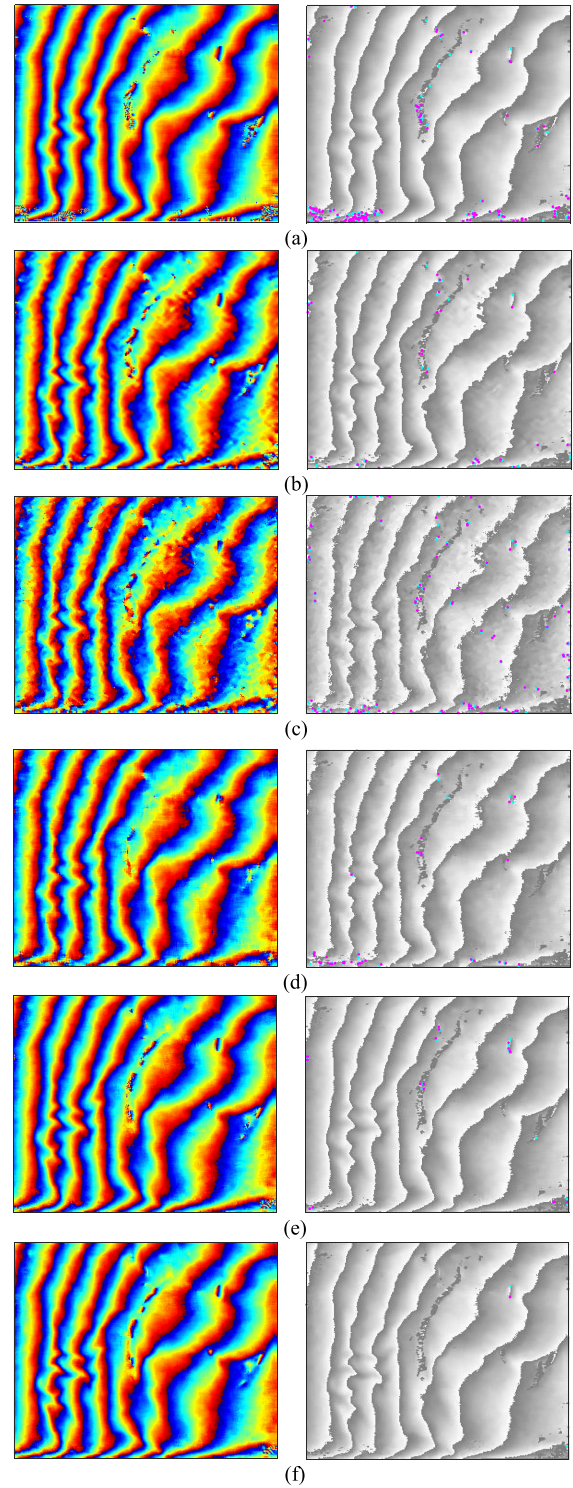


Fig. 13. Filtered phase and residues distribution. (a) Slope adaptive filtering. (b) Goldstein filtering. (c) NL-InSAR. (d) NL-SWAG. (e) Proposed method1. (f) Proposed method2.

the other four more or less cause some defects of phase detail and fringe breaks. Quantitative evaluation results are given in Table V. The areas affected by shadows are not included in the evaluation. Similar to the results of ERS data, the proposed method has demonstrated the least residues and the smallest

TABLE V
EVALUATION RESULTS OF NSAR DATA

Interferogram	Residues	RPSD	Time(s)
Noisy phase	14230	1.384	/
Slope adaptive filter	268	0.578	168
Goldstein filter	58	0.570	87
NL-InSAR	172	0.701	66
NL-SWAG	68	0.593	112
Proposed method1	38	0.508	226
Proposed method2	4	0.431	154

RPSD. Compared with local filtering methods, pixels in a larger range are used in nonlocal filters, which is beneficial to noise reduction; compared with other nonlocal filtering methods, after LFF compensation, the residual phase of the proposed method has sparser fringes, which helps with edge protection. Therefore, the proposed methods not only reduce the phase noise more effectively but also preserves the local fringe better.

IV. CONCLUSION

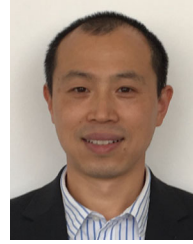
To improve the similarity matching ability of traditional NL-InSAR in areas with dense fringe, a new nonlocal noise suppression method has been proposed, which consists of three main steps. First, the local fringe compensation technique is employed to reduce fringe density; then, nonlocal filtering is implemented in the complex domain of the residual phase; finally, the denoised phase is obtained by combining the local fringes with the filtered residual phase. In addition, the smoothing parameter is improved based on statistical characteristics of the interferometric phase. As shown by filtering results using both simulated and real data, in the complex region, existing filtering methods suffer from different degrees of residual noise and loss of fringe detailed information, while the proposed one has achieved the best denoising and fringe preserving result.

Nonlocal filtering can find similar pixels in a larger range to suppress noise. However, the larger the search window, the more difficult to accurately estimate the LFF. One possible direction for future research is to realize the adaptive selection of similarity window and search window according to the fringe distribution of the residual phase, so as to further improve the adaptability of this method to steep terrains.

REFERENCES

- [1] E. Rodriguez and J. M. Martin, "Theory and design of interferometric synthetic aperture radars," *IEEE Proc. F-Radar Signal Process.*, vol. 139, no. 2, pp. 147–159, Apr. 1992.
- [2] R. Bamler and P. Hartl, "Synthetic aperture radar interferometry," *Inverse Probl.*, vol. 14, no. 4, pp. R1–R54, 1998.
- [3] D. Rife and R. R. Boorstyn, "Single tone parameter estimation from discrete-time observations," *IEEE Trans. Inf. Theory*, vol. IT-20, no. 5, pp. 591–598, Sep. 1974.
- [4] R. M. Goldstein and C. L. Werner, "Radar interferogram filtering for geophysical applications," *Geophys. Res. Lett.*, vol. 25, no. 21, pp. 4035–4038, Nov. 1998.
- [5] J. S. Lee, K. P. Papathanassiou, T. L. Ainsworth, M. R. Grunes, and A. Reigber, "A new technique for noise filtering of SAR interferometric phase images," *IEEE Trans. Geosci. Remote Sens.*, vol. 36, no. 5, pp. 1456–1465, Sep. 1998.
- [6] N. Wu, D. Feng, and J. Li, "A locally adaptive filter of interferometric phase images," *IEEE Geosci. Remote Sens. Lett.*, vol. 3, no. 1, pp. 73–77, Jan. 2006.
- [7] Q. Yu, X. Yang, and S. Fu, "An adaptive contoured window filter for interferometric synthetic aperture radar," *IEEE Geosci. Remote Sens. Lett.*, vol. 4, no. 1, pp. 23–26, Jan. 2007.
- [8] G. Vasile, E. Trouve, Jong-Sen Lee, and V. Buzuloiu, "Intensity-driven adaptive-neighborhood technique for polarimetric and interferometric SAR parameters estimation," *IEEE Trans. Geosci. Remote Sens.*, vol. 44, no. 6, pp. 1609–1621, Jun. 2006.
- [9] E. Trouve, J. M. Nicolas, and H. Maitre, "Improving phase unwrapping techniques by the use of local frequency estimates," *IEEE Trans. Geosci. Remote Sens.*, vol. 36, no. 6, pp. 1963–1972, Nov. 1998.
- [10] Z. Suo, Z. Li, and Z. Bao, "A new strategy to estimate local fringe frequencies for InSAR phase noise reduction," *IEEE Geosci. Remote Sens. Lett.*, vol. 7, no. 4, pp. 771–775, Oct. 2010.
- [11] Z. Ding, Z. Wang, S. Lin, T. Liu, Q. Zhang, and T. Long, "Local fringe frequency estimation based on multifrequency InSAR for phase-noise reduction in highly sloped terrain," *IEEE Geosci. Remote Sens. Lett.*, vol. 14, no. 9, pp. 1527–1531, Sep. 2017.
- [12] H. Xu, Q. Feng, Y. You, Z. Wu, W. Liu, and S. Ge, "Improved goldstein interferogram filter based on local fringe frequency estimation," *Sensors*, vol. 16, no. 11, 2016, Art. no. 1976. doi: 10.3390/s16111976.
- [13] D. Meng, V. Sethu, E. Ambikairajah, and L. Ge, "A novel technique for noise reduction in InSAR images," *IEEE Geosci. Remote Sens. Lett.*, vol. 4, no. 2, pp. 226–230, Apr. 2007.
- [14] A. Buades, B. Coll, and J. M. Morel, "A nonlocal algorithm for image denoising," in *Proc. IEEE Comput. Soc. Conf. Comput. Vis. Pattern Recognit.*, vol. 2, 2005, pp. 60–65, doi: 10.1109/CVPR.2005.38.
- [15] A. Buades, B. Coll, and J. M. Morel, "A review of image denoising algorithms with a new one," *Multiscale Model. Simul.*, vol. 4, no. 2, pp. 490–530, 2005.
- [16] C. A. Deledalle, L. Denis, and F. Tupin, "NL-InSAR: Nonlocal interferogram estimation," *IEEE Trans. Geosci. Remote Sens.*, vol. 49, no. 4, pp. 1441–1452, Apr. 2011.
- [17] A. Buades, B. Coll, and J. M. Morel, "Nonlocal image and movie denoising," *Int. J. Comput. Vis.*, vol. 76, no. 2, pp. 123–139, Feb. 2008.
- [18] G. Baier, C. Rossi, M. Lachaise, X. X. Zhu, and R. Bamler, "A nonlocal InSAR filter for high-resolution DEM generation from TanDEM-X interferograms," *IEEE Trans. Geosci. Remote Sens.*, vol. 56, no. 11, pp. 6469–6483, Nov. 2018.
- [19] X. Lin, F. Li, D. Meng, D. Hu, and C. Ding, "Nonlocal SAR interferometric phase filtering through higher order singular value decomposition," *IEEE Geosci. Remote Sens. Lett.*, vol. 12, no. 4, pp. 806–810, Apr. 2015.
- [20] D. Fang, X. Lv, and B. Lei, "A novel InSAR phase denoising method via nonlocal wavelet shrinkage," in *Proc. IEEE Int. Geosci. Remote Sens. Symp.*, 2016, pp. 6429–6432.
- [21] J. S. Lee, K. W. Hoppel, S. A. Mango, and A. R. Miller, "Intensity and phase statistics of multi-look polarimetric and interferometric SAR imagery," *IEEE Trans. Geosci. Remote Sens.*, vol. 32, no. 5, pp. 1017–1028, Sep. 1994.
- [22] Lin X *et al.*, "An adaptive iterated nonlocal interferometry filtering method," *J. Radars*, vol. 3, no. 2, pp. 166–175, Apr. 2014.
- [23] X. Yang and D. A. Clausi, "Structure-preserving speckle reduction of SAR images using nonlocal means filters," in *Proc. 16th IEEE Int. Conf. Image Process.*, 2009, pp. 2985–2988.
- [24] R. Hanssen, *Radar Interferometry: Data Interpretation and Error Analysis*. The Netherlands, Dordrecht: Kluwer, 2001.
- [25] U. Spagnolini, "2-D phase unwrapping and instantaneous frequency estimation," *IEEE Trans. Geosci. Remote Sens.*, vol. 33, no. 3, pp. 579–589, May 1995.
- [26] B. Cai, D. Liang, and Z. Dong, "A new adaptive multiresolution noise-filtering approach for SAR interferometric phase images," *IEEE Geosci. Remote Sens. Lett.*, vol. 5, no. 2, pp. 230–266, Apr. 2008.
- [27] Q. Wang, H. Huang, A. Yu, and Z. Dong, "An efficient and adaptive approach for noise filtering of SAR interferometric phase images," *IEEE Geosci. Remote Sens. Lett.*, vol. 8, no. 6, pp. 1140–1144, Nov. 2011.
- [28] R. Lanari, S. Hensley, and P. A. Rosen, "Chirp z-transform based SPECAN approach for phase-preserving ScanSAR image generation," *IEE Proc., Radar, Sonar Navig.*, vol. 145, no. 5, pp. 254–261, Oct. 1998.
- [29] D. Zhu and Z. Zhu, "Improving the coherence for InSAR processing and coherence estimation using the linear phase model," *Acta Electronica Sinica*, vol. 33, no. 9, pp. 1594–1599, 2005.

- [30] C. Cheng, F. Cheng, S. Huang, and B. Chen, "Integral nonlocal means algorithm for image noise suppression," *Electron. Lett.*, vol. 51, no. 19, pp. 1494–1495, 2015.
- [31] G. Franceschetti, A. Iodice, M. Migliaccio, and D. Riccio, "A novel across-track SAR interferometry simulator," *IEEE Trans. Geosci. Remote Sens.*, vol. 36, no. 3, pp. 950–962, May 1998.
- [32] S. Li, H. Xu, S. Gao, W. Liu, C. Li, and A. Liu, "An interferometric phase noise reduction method based on modified denoising convolutional neural network," *IEEE J. Sel. Topics Appl. Earth Observ. Remote Sens.*, vol. 13, pp. 4947–4959, 2020.
- [33] J. Li, Z. Li, Z. Bao, Y. Hou, and Z. Suo, "Noise filtering of high-resolution interferograms over vegetation and urban areas with a refined nonlocal filter," *IEEE Geosci. Remote Sens. Lett.*, vol. 12, no. 1, pp. 77–81, Jan. 2015.
- [34] A. Liu, F. Wang, and H. Xu, "N-SAR system: First demonstration of flight test results," in *Proc. 12th Eur. Conf. Synthetic Aperture Radar*, 2018, pp. 1–4.
- [35] I. Baran, M. P. Stewart, B. M. Kampes, Z. Perski, and P. Lilly, "A modification to the Goldstein radar interferogram filter," *IEEE Trans. Geosci. Remote Sens.*, vol. 41, no. 9, pp. 2114–2118, Sep. 2003.



Wei Liu (Senior Member, IEEE) received the B.Sc. and L.L.B. degrees in space physics from Peking University, China, in 1996 and 1997, respectively, MPhil from the Department of Electrical and Electronic Engineering, University of Hong Kong in 2001, and PhD from the School of Electronics and Computer Science, University of Southampton, UK, in 2003.

He later worked as a Postdoc with Imperial College London. Since September 2005, he has been with the Department of Electronic and Electrical Engineering, University of Sheffield, Sheffield, U.K., as a Lecturer, and then a Senior Lecturer. He has authored or coauthored more than 250 journal and conference papers, three book chapters, and a research monograph about wideband beamforming. His research interests include sensor array signal processing, blind signal processing, multirate signal processing, and their various applications in wireless communications, radar, sonar, satellite navigation, human-computer interface, and renewable energy exploitation.

Dr. Liu is an elected member of the Digital Signal Processing Technical Committee of the IEEE Circuits and Systems Society, currently an Associate Editor for the IEEE TRANSACTIONS ON SIGNAL PROCESSING and IEEE ACCESS, and an Editorial Board Member of the *Journal Frontiers of Information Technology and Electronic Engineering*.



Huaping Xu received the B.S. degree in electronic engineering and the Ph.D. degree in communication and information system from Beihang University, Beijing, China, in 1998 and 2003, respectively.

She is currently with the School of Electronic and Information Engineering, Beihang University. Her current research include SAR, SAR interferometry, differential SAR interferometry, and SAR image processing using advanced signal processing method.



Jingwen Li received the M.S. degree in signal and information processing and Ph.D. degree in communication and information system from Beihang University, Beijing, China, in 1988 and 1999, respectively.

Since 2000, he has been a Professor with the School of Electronic and Information Engineering, Beihang University. His current research interests include synthetic aperture radar (SAR) image processing, new SAR system design, and SAR ground moving target indication methods.



Zhaohong Li received the B.S. degree in photoelectric engineering from the Changchun University of Science and Technology, Changchun, China, in 2016, and the M.S. degree in electrical and electronic engineering from The University of Sheffield, Sheffield, U.K., in 2017. He is currently working toward Ph.D. degree in signal and information processing from Beihang University, Beijing, China.

His research interests include target detection for multiband SAR image and SAR interferometry processing.



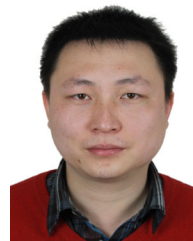
Aifang Liu received the B.S. degree in electronic engineering from Shanxi University, Taiyuan, China, in 1997, the M.S. and Ph.D. degrees in communication and information system from Nanjing University of Science and Technology, Nanjing, China, in 2001 and 2004, respectively.

He is currently working in the Nanjing Research Institute of Electronics Technology, and is mainly engaged in the design of space-based radar system and synthetic aperture radar system.



Shuo Li received the M.S. degree in electronic science and technology from China University of Mining and Technology in 2015. He is currently working toward Ph.D. degree in signal and information processing from Beihang University, Beijing, China.

His research interests include SAR image processing, SAR interferometry processing, especially registration, and phase unwrapping.



Wei Li received the Ph.D. degree in signal and information processing from Beihang University, Beijing, China, in 2011.

He is currently a Senior Engineer with the Shanghai Institute of Satellite Engineering, Shanghai, China. He is also currently a member of the National Space Infrastructure Demonstration Group and Secretary General of the Secretariat of the Civil P-Band Satellite Scientists Committee. His main research interests include satellite system design and system performance analysis.